A NEMO-based model of *Sargassum* distribution in the Tropical Atlantic: description of the model and sensitivity analysis (NEMO-Sarg1.0)

Julien Jouanno[1], Rachid Benshila[1], Léo Berline[2], Antonin Soulié[1], Marie-Hélène Radenac[1], Guillaume Morvan[1], Frédéric Diaz[2], Julio Sheinbaum[3], Cristele Chevalier[2], Thierry Thibaut[2], Thomas Changeux[2], Frédéric Menard[2], Sarah Berthet[4], Olivier Aumont[5], Christian Ethé[5], Pierre Nabat[4], Marc Mallet[4].

[1] LEGOS, Université de Toulouse, IRD, CNRS, CNES, UPS, Toulouse, France
[2] Aix-Marseille University, Université de Toulon, CNRS/INSU, IRD, MIO UM 110, Mediterranean Institute of Oceanography (MIO), Campus of Luminy, 13288 Marseille, France
[3] CICESE, Ensenada, Mexico.
[4] CNRM, Université de Toulouse, Météo-France, CNRS, Toulouse, France
[5] Laboratoire d'Océanographie et de Climatologie: Expérimentation et Approches Numériques, IRD-IPSL, 4 Place Jussieu, 75005 Paris, France

Correspondence to: Julien Jouanno (julien.jouanno@ird.fr)

Abstract. The Tropical Atlantic is facing a massive proliferation of Sargassum since 2011, with severe environmental and socioeconomic impacts. The development of Sargassum modelling is essential to clarify the link between Sargassum distribution and environmental conditions, and to lay the groundwork for a seasonal forecast on the scale of the Tropical Atlantic basin. We developed a modelling framework based on the NEMO ocean model, which integrates transport by currents and waves, physiology of Sargassum with varying internal nutrients quota, and considers stranding at the coast. The model is initialized from basin scale satellite observations and performance was assessed over the Sargassum year 2017. Model parameters are calibrated through the analysis of a large ensemble of simulations, and the sensitivity to forcing fields like riverine nutrients inputs, atmospheric deposition, and waves is discussed. Overall, results demonstrate the ability of the model to reproduce and forecast the seasonal cycle and large-scale distribution of Sargassum biomass.

1 Introduction

The massive development of holopelagic *Sargassum* spp. in the Northern Tropical Atlantic Ocean from 2011 causes annual stranding in millions of tons on the coasts of the Lesser Antilles, Central America, Brazil and West Africa (e.g., Smetacek and Zingone 2013, Wang and Hu 2016, Langin 2018, Wang et al. 2019). The proliferation affects the whole northern Tropical Atlantic area as illustrated by satellite observations for summer 2017 (Figure 1, Berline et al. 2020).

Modelling and forecasting the *Sargassum* proliferation and strandings is essential for designing effective integrated risk management strategies, and is a strong and pressing demand from the civil society. This operational challenge concerns both event forecasts (i.e., on a one-week scale) and long-term forecasts (one to several months). While many efforts have been made for short-term forecast, initiatives for reliable long-term forecasting are very scarce and face several scientific challenges such

35   as the large uncertainties in *Sargassum* detection and biomass quantification (Wang et al. 2018, Ody et al. 2019), a lack of knowledge on *Sargassum* physiology, and last but not least the absence of tools specifically designed to reproduce the large-scale distribution and evolution of these macro-algae.

Recent studies suggest that the increasing incidence of *Sargassum* blooms and its year-to-year variability is multifactorial: it may result from riverine and atmospheric fertilization of the upper ocean, West Africa upwelling variability, vertical

40   exchanges at the mixed-layer base in the region of the Inter-Tropical Convergence Zone, ITCZ) or anomalous transport due to climate variability (Oviatt et al. 2018, Wang et al. 2019, Johns et al. 2020). This highlights the complexity of the phenomenon and the need for a basin-scale and inter-disciplinary approach.

In the recent years, modelling effort mainly focused on the transport properties of *Sargassum* rafts by offshore currents (Wang and Hu, 2017, Brooks et al. 2018, Maréchal et al., 2017, Putman et al 2018, 2020, Wang et al. 2019, Berline et al. 2020,

45   Beron-Vera and Miron, 2020), with significant advances on the role of inertia in the drift trajectories (Brooks et al. 2019, Beron-Vera and Miron 2020) and the importance of considering windage to properly resolve the drift of the *Sargassum* mats (Putman et al. 2020, Berline et al. 2020). To our knowledge, Brooks et al. (2018) were the first to integrate *Sargassum* physiology along the trajectories and showed that considering growth and mortality improved the modelling of the large-scale distribution of *Sargassum*. A similar result was obtained in Wang et al. (2019), although they did not consider directly the

50   physiology of the algae but local growth rate based on satellite observations. Indeed, few studies have investigated the biology and ecology of this holopelagic *Sargassum* species that proliferate in the Atlantic and their response to the variability of environmental parameters (Lapointe 1995, 1986, Hanisak and Samuel 1987, Carpenter and Cox 1974, Hanson 1977, Howard and Menzies 1969).

In the present paper, we describe the numerical model we developed to represent the distribution of holopelagic *Sargassum*.

55   This model relies on an Eulerian approach and integrates both transport and a simplified physiology model of the macroalgae. It is based on the NEMO modelling system, which is widely used by the research community and European ocean forecasting centers (*e.g.*, Mercator Ocean International, ECMWF), allowing efficient parallelization and interfacing with physical-biogeochemical models. In the following section, we review current knowledge on the ecology of *Sargassum*. The modelling system is described in section 3. Section 4 shows the performance of the model at seasonal scale and discusses sensitivity of

60   the modeled *Sargassum* distribution to the forcing fields. Discussion and a summary are given in the final Section.

2 Physiological and ecological features of holopelagic *Sargassum*

Pelagic *Sargassum* species (to date *Sargassum natans* and *S. fluitans*) are brown algae (Phaeophyceae) that live at the surface of the ocean, never attached to any substrate. Within these two taxonomic groups, three types of *Sargassum* that can be distinguished according to morphological features, appear to fuel the recent *Sargassum* inundations in the Caribbean: *S. fluitans* III, *S. natans* I, *S. natans* VIII (Schell et al 2015). We still lack knowledge on the distribution of these species, but in recent years, *S. fluita*ns III was predominant in 2017 (Ody et al., 2019) and form beaching on the Yucatan Coast, comprising on average >60 % of total wet biomass (Garcia Sanchez et al. 2020), whereas Schell et al. (2015) reported a predominance of *S. natans* VIII in 2015.

One individual *Sargassum* fragment can vary in length from just one cm to more than 1 m. Under the action of Langmuir cells and ocean currents, *Sargassum* tends to group together to form large floating rafts at the water surface (e.g., Langmuir 1936, Zhong et al. 2012). Individuals in these aggregations can be easily dispersed by wind, waves or any event (Ody et al., 2019). These assemblages spread out horizontally and can reach several tens of km and a few meters thick.

Biological and physiological features are species dependent. We know relatively little about the physiology of these *Sargassum*. Considering biomass, their maximum growth rate is estimated to be around 0.1 d^{-1} (Lapointe 1986, Hanisak and Samuel 1987, Lapointe et al. 2014). The *Sargassum* growth is sensitive to light and temperature. Carpenter and Cox (1974) suggest light saturation under normal October light conditions in the Sargasso Sea (35 W m^{-2}), while Hanisak and Samuel (1987) found a higher saturation range of ~43-65 W m^{-2}. The temperature dependence in Hanisak and Samuel (1987) for *Sargassum natans* suggests a broad optimal temperature range of 18-30°C and indicates no growth at 12°C. We lack information on *Sargassum fluitans* response to the variability of the environmental parameters.

Lapointe (1986) highlights a growth mainly limited by phosphate availability, while the presence of nitrifying epiphytes (Carpenter 1972, Michotey et al. 2020) could be a non-negligible source of nitrogen for *Sargassum*, as could urea and ammonium excreted by fish (Lapointe et al. 2014). It is also likely that *Sargassum* are able to store some nutrients in their tissues, as do other brown algae (e.g., Hanisak 1983). This hypothesis is supported by Lapointe et al. (1995) whose measurements revealed variable elemental compositions between individuals sampled in neritic *vs* oceanic waters. In addition, no macro-herbivores control holopelagic development offshore by grazing (Butler et al. 1983).

3 The *Sargassum* modelling framework

Our modelling strategy relies on a physical-biogeochemical model that resolves currents and nutrient variability in the Atlantic. We choose to develop a regional configuration so the model can be tuned to the region specificity and can be used to perform sensitivity tests as discussed in Section 4. In addition, our approach is based on a *Sargassum* model that integrates transport, stranding and physiology of the macroalgae in the ocean surface layer, forced with surface fields obtained from the physical-biogeochemical model.

The two models share the same horizontal domain and grid, and are both based on the NEMO modelling system version 4.0 (Nucleus for European Modelling of the Ocean, Madec et al. 2016). They are not coupled assuming then that *Sargassum* does not compete with phytoplankton (and heterotrophic bacteria) for nutrient resources, and that they are not grazed by the

95 herbivore compartments of the biogeochemical model.

3.1 The physical-biogeochemical model TATL025BIO

For the physical component of the simulation, we use the regional NEMO-based configuration described in Hernandez et al. (2016, 2017) and Radenac et al. (2020) that covers the tropical Atlantic between 35°S and 35°N and from 100°W to 15°E. The resolution of the horizontal grid is ¼° and there are 75 vertical levels, 24 of which are in the upper 100 m of the ocean. The

100 depth interval ranges from 1 m at the surface to about 10 m at 100 m depth. Interannual atmospheric fluxes of momentum, heat, and freshwater are derived from the DFS5.2 product (Dussin et al., 2016) using bulk formulae from Large and Yeager (2009). Temperature, salinity, currents, and sea level from the MERCATOR global reanalysis GLORYS2V4 (Storto et al., 2018) are used to force the model at the lateral boundaries.

The physical model is coupled to the PISCES (Pelagic Interaction Scheme for Carbon and Ecosystem Studies)
105 biogeochemical model (Aumont et al., 2015) that simulates the biological production and the biogeochemical cycles of carbon, nitrogen, phosphorus, silica, and iron. We use the PISCES-Q version with variable stoichiometry described in Kwiatkowski et al. (2018), and with an explicit representation of three phytoplankton size classes (picophytoplankton, nanophytoplankton and microphytoplankton) and two zooplankton compartments (nanozooplankton and mesozooplankton). The model also includes three non-living compartments (dissolved organic matter and small and large sinking particles). The biogeochemical model is
110 initialized and forced at the lateral boundaries with dissolved inorganic carbon, dissolved organic carbon, alkalinity, and iron obtained from stabilized climatological 3-D fields of the global standard configuration ORCA2 (Aumont and Bopp, 2006), and nitrate, phosphate, silicate, and dissolved oxygen from the World Ocean Atlas observation database (WOA; Garcia et al., 2010). The model is run from 2006 to 2017 and daily fields are extracted to force the *Sargassum* model.

Particular care has been given to the prescription of the atmospheric and riverine fluxes of nutrients. The river runoffs
115 are based on daily fluxes from the ISBA-CTRIP reanalysis (Decharme et al. 2019) which has proven to accurately reproduce the interannual variability of the large rivers of the basin (e.g., see Giffard et al. 2019 for the Amazon river). The riverine nutrient fluxes concentrations are from the GLOBAL-NEWS2 dataset, corrected with *in situ* observations from the Amazon basin water resources observatory database (HYBAM, https://hybam.obs-mip.fr/) for the Amazon, Orinoco and Congo rivers. As in Aumont et al. (2015), we consider an atmospheric supply of P, Fe and Si from dust deposition. Here, these fluxes are
120 forced using monthly dry-plus-wet deposition products (DUDPWTSUM) from the MERRA-2 data available on the NASA Giovanni website (http://disc.sci.gsfc.nasa.gov/giovanni). Comparison with *in situ* observations of dust fluxes in Guyana and in Barbados lead to an excellent match with MERRA2 fluxes (Prospero et al. 2020). A climatological deposit of N is obtained from global climate simulations carried out with the ARPEGE-Climate model (Michou et al. 2020). An interactive aerosol

scheme including nitrate and ammonium particles (Drugé et al. 2019) is included in ARPEGE-Climate, allowing us to produce
125   fields of wet and dry deposition of nitrogen, ammonium and ammonia. Figure 2 illustrates that dust and nitrogen fluxes to the
ocean are strong in our region of interest, and most particularly in the ITCZ region where atmospheric convergence may focus
the wet fluxes.

The modeled chlorophyll for year 2017 is compared with GLOBCOLOUR satellite estimates of chlorophyll for the same
year (Figure 3a,b). Model NO_3 and PO_4 concentrations for 2017 are compared with historical *in situ* measurements (Figure 3c-
130   f) from the GLODAPV2 database (Olsen et al., 2016). The model reproduces the major chlorophyll structures and in particular
the contrast between the oligotrophic subtropical gyre and productive coastal and equatorial upwellings (Figures 3a, b). As
many other models (*e.g.,* see the CMIP6 model evaluation by Seferian et al. 2020), it struggles to reproduce the offshore extent
of the large river plumes and Guinea dome productivity. Moreover, coastal upwellings tend to be too productive offshore or
downstream (for the equatorial upwelling). But above all, it represents realistically the chlorophyll distribution in the region
135   of the ITCZ (~0-10°N) and in the Caribbean Sea. As observed, nitrate concentrations are high in the upwelling areas (Figures
3c, d) but weaker than observed off these regions. It is worth noticing that historical observations of surface nitrate
concentrations in the tropical band show very heterogeneous and contrasted values between cruises, so the reliability of a
nitrate climatology in this area remains uncertain (Figure 3c). The model reproduces realistically the observed interhemispheric
gradient of surface phosphate concentrations even though it likely overestimates areas of high phosphate contents (Figures 3e,
140   f).

3.2 The *Sargassum* model NEMO-Sarg1.0

The *Sargassum* model relies on the strategy used to represent the distribution of other macroalgae species (*e.g.*, Martin and
Marques 1993, Solidoro et al. 1997, Perrot et al. 2014 or Ren et al. 2014). At the difference of these previous works, we also
consider transport by 2D advection/diffusion equations and sink due to stranding at the coast. Growth is modeled as a function
145   of internal reserves of nutrients, dissolved inorganic nutrients in the external medium, irradiance and sea temperature. As the
eco-phycological features are species dependent, the actual knowledge on the three morphotypes of holopelagic *Sargassum*
does allow to discriminate between them. Following the formalism given in Ren et al. (2014), the physiological behavior is
described from three state variables: the contents in carbon (C), nitrogen (N) and phosphorus (P), with local variations
reflecting the difference between uptake and loss rates.

150

$$\frac{\partial C}{\partial t} = U_C - \phi_C$$

$$\frac{\partial N}{\partial t} = U_N - \phi_N$$

$$\frac{\partial P}{\partial t} = U_P - \phi_P$$

5

155   where U_C, U_N and U_P are the uptake rates of carbon, nitrogen and phosphorus respectively, and Φ_C, Φ_N, Φ_P the loss rates.

The rate of carbon uptake reads as follows: $U_c = C \cdot \mu_{max} \cdot f[T] \cdot f[I] \cdot f[Qn] \cdot f[Qp]$, with μ_{max} the maximum net carbon growth rate, and the four subsequent terms standing for uptake limitation by temperature (T), solar radiation (I), N-quota (Qn), and P-quota (Qp), respectively. N and P quotas represent the ratios of nitrogen and phosphorus to carbon in the organism and are computed as N/C and P/C respectively. The C content (C) can be directly converted to dry biomass

160   considering a mean carbon to dry weight ratio of 27% (Wang et al. 2018).

The temperature dependence is adapted from Martins and Marques (2002):

$$f(T) = e^{-\frac{1}{2}\left(\frac{T-Topt}{T_x-T}\right)^2}$$

165

with $\{T_x = T_{min} \; for \; T \leq T_{opt} \; ; \; T_x = T_{max} \; for \; T > T_{opt}\}$. T_{opt} is the optimum temperature at which growth rate is maximum, T_{min} is the lower temperature limit below which growth ceases, T_{max} is the upper temperature limit above which growth ceases. Such function aims at representing a broad optimal temperature range as suggested by experiments in Hanisak and Samuel (1987). The dependence to light follows the function given in Martins and Marquez (2002) with photoinhibition

170   at high light:

$$f(I) = \frac{I}{I_{opt}} \cdot e^{\left(1-\frac{I}{I_{opt}}\right)}$$

We have very few information on the response curve relating the nutrient quota to *Sargassum* growth but experiments for brown seaweeds suggest hyperbolic relationship (*e.g.*, Hanisak 1983). So, the dependence to the internal nitrogen and

175   phosphorus pools are computed as a hyperbolic curve controlled by the minimum and maximum cell quota:

$$f(Q_N) = \left(\frac{1 - Q_{Nmin}/Q_N}{1 - Q_{Nmin}/Q_{Nmax}}\right)$$

$$f(Q_P) = \left(\frac{1 - Q_{Pmin}/Q_P}{1 - Q_{Pmin}/Q_{Pmax}}\right)$$

180   The nitrogen and phosphorus uptake rates depend on the nitrogen (V_{Nmax}) and phosphorus (V_{Pmax}) maximum uptake velocities, a Monod kinetic that relates uptake to nutrient concentrations in the water, and a function of quota which aims at representing downregulation of the transport system for N and P when approaching the maximum quotas (Lehman et al. 1975):

$$U_N = V_{Nmax} \cdot C \cdot \left(\frac{[N]}{K_N + [N]} \right) \cdot (\frac{Q_{Nmax} - Q_N}{Q_{Nmax} - Q_{Nmin}})$$

$$U_P = V_{Pmax} \cdot C \cdot \left(\frac{[P]}{K_P + [P]} \right) \cdot (\frac{Q_{Pmax} - Q_P}{Q_{Pmax} - Q_{Pmin}})$$

185

The carbon loss aims at representing mortality, stranding and sinking:

$$\phi_C = C \cdot \left(\frac{m}{e^{-\lambda_m \cdot (T - 30°C)}} + \delta_{land} \cdot \alpha_{grnd} + \frac{m_{LC}}{e^{-\lambda_{mLC} \cdot (H_{LC} - 100m)}} \right).$$

190

The mortality term depends on m the mortality rate, λ_m a mortality coefficient, and temperature T. We thus represent thallus senescence and bacterial activity as a growing function of temperature (Bendoricchio et al. 1994, Ren et al., 2014).

The stranding is function of α_{grnd} which is a rate of *Sargassum* stranding per unit of time, and δ_{land} which is defined as follows:

195

$$\begin{cases} \delta_{land} = 1 \; if \; model \; grid \; cell \; is \; adjacent \; to \; two \; or \; more \; pixels \; of \; land, \\ \delta_{land} = 0 \; otherwise. \end{cases}$$

The sinking rate of *Sargassum* is estimated as a function of the Langmuir cell length scale H_{LC} and a sinking coefficient m_{LC}. The aim is to reproduce possible *Sargassum* loss by Langmuir cell as hypothesized by Johnson and Richardson (1977) or Woodcock (1993) to explain large amounts of *Sargassum* observed at the sea floor (Schoener and Rowe 1970, Baker et al. 2018). Following, Axel et al. (2014), we estimate H_{LC} as the depth that a water parcel with kinetic energy $u_s^2/2$ can reach on its own by converting its kinetic energy to potential energy. This corresponds to: $-\int_{-H_{LC}}^{0} N^2(z) \cdot z \cdot dz = \frac{1}{2} \cdot u_s^2$, with u_s the Stokes drift and N^2 the Brunt Vaisala frequency. We fixed a 100m depth threshold as *Sargassum* becomes massively negatively buoyant at these depths (Johnson and Richardson, 1977).

205

Losses of nitrate and phosphate are function of the loss of biomass and internal N and P quotas:

$$\phi_N = \phi_C \cdot Q_N \; , \phi_P = \phi_C \cdot Q_P \; .$$

210　The transport of C, N, and P is resolved using 2D advection/diffusion equations discretized on a grid at 1/4° resolution with a single vertical layer representing a surface layer of water of one-meter depth. The surface velocities used for the transport, account for surface currents, windage effect and wave transport by stokes drift:

$$\phi_{transport}(Nutrient) = -U \cdot \frac{\partial Nutrient}{\partial x} - V \cdot \frac{\partial Nutrient}{\partial y} + K_h \cdot \nabla_h^2 Nutrient, \text{ with}$$

215

$$U, V = (u_{NEMO}, v_{NEMO}) + \alpha_{win} \cdot (u_{10m}, v_{10m}) + (u_{Stokes}, v_{Stokes})$$

where (u_{NEMO},v_{NEMO}) are the horizontal velocity obtained from the physical-biogeochemical model, α_{win} is a windage coefficient, (u_{10m}, v_{10m}) the components of the wind field at 10m above the sea level, (u_{stokes},v_{stokes}) the stokes velocity, and K_h a diffusion coefficient.

220 **3.3 Optimization and sensitivity experiments**

The model simulations are performed for year 2017 because basin scale *Sargassum* fractional coverage observations from MODIS were available (Berline et al. 2020), with concurrent observations carried out during two cruises in the Tropical Atlantic (Ody et al. 2019).

3.3.1 Initialization

225 The simulations are initialized using January *Sargassum* mean fractional coverage, converted into dry weight biomass considering a surface density of 3.34 kg/m² and then into carbon content C considering a mean carbon to dry weight ratio of 27% (Wang et al. 2018). The initial N and P contents in *Sargassum* are derived from the initial C content and N- and P- quotas computed as the averaged values between their respective minimum values (Q_{Nmin}, Q_{Nmin}) and maximum values (Q_{Nmax}, Q_{Nmax}). The transport is forced by daily velocities from TATL025BIO simulations (see Section 3.1), 3-hours winds from the DFS5.2

230 dataset (Dussin et al. 2016) and stokes velocities from the ERA5 reanalysis. Daily temperature, available irradiation, and Langmuir depth were also obtained from TATL025BIO. The seawater concentrations in [N] and [P] were obtained from TATL025BIO as the sum of NO_3 and NH_4 for [N], and PO_4 for [P], in the top surface layer.

3.3.2 Ensemble strategy

The *Sargassum* model is controlled by a large number (n=18) of physiological and physical parameters for which large

235 uncertainties exist or most often have not been measured for the *Sargassum* species considered here. An ensemble approach has been adopted to adjust the set of parameters. We produced 10 000 sets of parameters with uniform distribution obtained from latin hypercube sampling with multi-dimensional uniformity (Deutsch and Deutsch, 2012). These sets of parameters are generated on ranges of values obtained from the literature, when available (Table 1).

The range of maximum growth rate is derived from Lapointe et al. (2014) who observed maximum growth rates of

240 *Sargassum fluitans* and *Sargassum natans* in neritic waters between 0.03 and 0.09 doubling d^{-1}. The set of parameters for temperature limitation is mainly derived from the results of Hanisak and Samuel (1987). In particular, the T_{max} range (40-50°C) is chosen to have a slight decrease of the limitation term at T>T_{opt} as observed in Hanisak and Samuel (1987). The N- and P-quota are based on the observations by Lapointe et al. (1995) from which we can estimate that in average C/N ratio vary

between 20 and 30 in neritic waters and between 40 and 70 in oceanic waters, while C/P ratios vary between 200 and 500 in
245   neritic waters and 700 and 1000 in oceanic waters. The lower and upper limit for the maximum nitrate uptake rate ($[5.0\ 10^{-4}$,
$1.3\ 10^{-3}]\ mg\ N\ (mg\ C)^{-1}\ d^{-1}$) is estimated from measurements by Lapointe et al. (1995). From this study we estimate
maximum carbon uptake rates in neritic water at ~2 mg C (g dry wt)$^{-1}$ h^{-1} with C/N ratio of 20, and maximum carbon uptake
rates in oceanic water at ~1 mg C (g dry wt)$^{-1}$ h^{-1} with C/N ratio of 60. Since the model does not take into account a diurnal
cycle of light, the maximum uptake has been divided by 3 in order to have a daily-mean maximum uptake. This ratio of 3 is
250   obtained by comparing instantaneous gross production at full irradiance vs. measured gross production from culturing the
Sargassum under natural irradiance in Lapointe et al. (2014). Similarly, the lower and upper limits for the maximum
phosphorus uptake rate ($[9\ 10^{-5}, 7\ 10^{-4}]\ mg\ N\ (mg\ C)^{-1}\ d^{-1}$) are estimated from measurements by Lapointe et al. (1995) which
give a C/P ratio of 200 in neritic waters and 800 in oceanic waters.

3.3.3 Likelihood function

255   The likelihood function (L) to be minimized is the Centered Root Mean Square error between monthly series of observed and
modeled *Sargassum* biomass contained in the North Tropical Atlantic Ocean, defined as [98°W-10°W, 0°-30°N], hereinafter
NTAO:

$$L = \left[\frac{1}{Nt} \sum_{t=1}^{Nt} [(\psi_m(t) - \overline{\psi_m}) - (\psi_{obs}(t) - \overline{\psi_{obs}})]^2 \right]^{1/2},$$

260

with Nt the number of outputs (12 months in our case), $\psi_m(t)$ and $\psi_{obs}(t)$ the modeled and observed biomass in the NTAO,
and the overbars designating the annual average.

The choice of this likelihood function exerts no constraints on the spatial distribution of the *Sargassum* and does not
consider uncertainties in the satellite measurements due to false detection, cloud masking, or *Sargassum* immersion. But as
265   shown in the following section, such a simple strategy allows to efficiently select a set of parameters that allow a good
representation of the seasonal *Sargassum* distribution.

3.3.4 Sensitivity analysis

Once a set of values minimizing *L* was found, one-at-a-time sensitivity experiments were also performed, where only one
single parameter is varied by ±10% in two model runs while the others are fixed (e.g., Ren et al. 2014, Perrot et al. 2014). This
270   allows to capture the direct contribution from each parameter to the output variance, with parameters varying within an
acceptable range. The set of values for the fixed parameters are given in Table 1 and were taken from the simulation with
higher *L*. Following Ren et al. (2014), deviation from the baseline simulation (D) is quantified as:

$$D = \frac{1}{N} \sum_{t=1}^{t=12} \frac{\psi_{m(i,t)} - \psi_{m(t)}^0}{\psi_{m(t)}^0}, \text{ with N=12}$$

275

where ψ_{mt}^0 refers to the simulated biomass in the NTAO from the baseline parameter set at month t, and $\psi_{m(i,t)}$ is the simulated biomass with one perturbed parameter i at month t. Two model runs were conducted with plus and minus 10% change to the baseline value.

4. Results

280 **4.1 Seasonal distribution and sensitivity to model parameters**

The observed and model seasonal distributions of *Sargassum* in 2017 are shown in Figure 4. Model distribution is obtained from the ensemble mean of the 100 simulations with the lowest *L*. Hereafter, this ensemble will be referred to as Ω_{100}. Averages over selected areas are shown in Figure 5. At this stage, it is worth recording that the selection of the ensemble simulations is performed without constraints on the spatial distribution, the only constraint being on the basin scale seasonal biomass average

285 (*L*).

Initialized in January, the model reproduces the seasonal distributions of *Sargassum* fairly closely. It simulates the *Sargassum* drift toward the Caribbean Sea, with a summer peak of biomass followed by a decrease until the end of the year, although the increase of biomass comes a little too early in February-March. In the Caribbean Sea, the largest abundance of *Sargassum* in the Northern part of the basin near the Greater Antilles compared to the South of the Caribbean is consistent

290 with observations. Despite a bloom that is occurring too early (May-June) near the Lesser Antilles, the modelled seasonal cycle is also consistent with the observations in this area (Figure 5b). This is encouraging from the perspective of predicting strandings on the Caribbean islands. It also succeeds in maintaining the biomass in the Eastern part of the North Tropical Atlantic below the ITCZ (Figure 4 and 5d). In the Sargasso Sea area (Figure 5c), simulations and observations consistently show an increase at the end of the year.

295 The distribution of parameters for the ensemble Ω_{100} is given in Figure 6. There is a significant dispersion of most of the parameters, suggesting either low sensitivity to the parameters in question (as discussed below) or interdependency between them. The analysis shows that there are very different sets of parameters, within the prescribed ranges, that lead to similar seasonal biomass distribution. (Figure 5). Having said that, we observe that the mortality parameters m and λ_m minimizing L are biased toward low and high values, respectively. This highlights the key importance of this mortality function in

300 representing the seasonal distribution. The nitrogen half-saturation constant K_N and the maximum uptake rate of nitrogen V_{Nmax} are also distributed toward low and high values, respectively, suggesting some sensitivity of the *Sargassum* distribution to nitrogen resources. These parameters are poorly constrained by observations and such exercise will allow us to refine the optimization ranges for future studies.

The relative mean deviation of the *Sargassum* seasonal biomass to 10% variations in model parameters shown in Figure 7
305 confirms findings from the analysis of parameter dispersion in Figure 6. The most influential parameters are the growth rate,
mortality dependence to temperature, and parameter controlling the nitrogen uptake V_{Nmax}. It also highlights the influence of
the minimum N-quota (Q_{Nmin}). There is moderate dependence on temperature and light, which is in good agreement with
measurements from Hanisak and Samuel (1987). In agreement with previous Lagrangian studies (Berline et al. 2020, Putman
et al. 2020), we find some sensitivity to the windage parameter.

310 The simulated stranding from the ensemble Ω_{100} is shown in Figure 8. At the scale of the Tropical Atlantic, these stranding
sum to 1.05 million tons dry weight for the whole year. The predicted strandings in the Caribbean, Northern Brazil, French
Guiana, Sierra Leone, correspond with our current knowledge of *Sargassum* invasions (Bernard et al., 2019; Louime et al.,
2017; Oviatt et al., 2019; Sissini et al., 2017; Oyesiku and Egunyomi 2014, Smetacek and Zingone, 2013). Nevertheless, there
are no available large-scale coastal observations or estimates of stranding to go further in the validation of these simulated
315 stranding.

A peculiarity of our modelling strategy is to consider the Stokes drift. The Stokes drift induces a displacement of material
parallel to the direction of wave propagation which directly transports the *Sargassum*. An ensemble of 100 simulations without
Stokes drift ("*NoStokes*"), considering the set of physiological parameters from Ω_{100}, has therefore been conducted. Anomalies
of annual *Sargassum* distribution with respect to Ω_{100} are shown in Figure 9a. *Sargassum* coverage is significantly increased
320 in the Central Atlantic but decreases sharply in the Caribbean and the Southwestern part of the domain. This highlights the
influence of waves, most probably due to the trade winds, in shaping the seasonal distribution, and transporting the algae
southward.

4.2 Sensitivity to external nutrient forcing

We now use the *Sargassum* model to explore how and to which extent continental nutrient sources (riverine nutrient fluxes,
325 dust deposition, atmospheric N deposition) could participate in the proliferation and may shape the seasonal distribution of
Sargassum. First, TATL025BIO simulations were run by deactivating the river sources (simulation "*noriver*"), atmospheric
deposition of P, Si Fe (simulation "*nodust*") or atmospheric deposition of N (simulations "*noNdepo*"). We choose to distinguish
between dust and N deposition because they have not the same origin and because spatial, seasonal and long-term variability
are not necessarily the same. The simulations were produced from 2006 so the long-term influence of these forcing on the
330 biogeochemical content is considered there. These simulations were then used to force three ensembles of 100 simulations
which used the sets of parameters from Ω_{100}.

As expected for the "*noriver*" ensemble, the Western Tropical Atlantic, which is under influence of the Amazon and
Orinoco rivers, is experiencing a decrease in nutrient concentrations (Figure 10b). Nutrients also show a decrease in the
Equatorial Atlantic. But for other regions, such as the Sargasso Sea or the Guinea Dome, the long-term equilibration results in
335 an increase in nitrogen concentration. The resulting *Sargassum* coverage shows a negative anomaly in the Caribbean Sea, in

the Gulf of Mexico and in the region of the ITCZ, with an annual mean basin scale biomass decrease (Figure 9a). For this ensemble, strandings are decreased from 1.05 Mt to 0.78Mt (-25%).

The "*nodust*" ensemble *Sargassum* distribution shows a slight positive anomaly over most of the domain (Figure 9c), particularly in the Central Atlantic and off West Africa, with a slight decrease in the Caribbean Sea and the Gulf of Mexico.

340 Cumulative strandings sum to 1.1 Mt, and so, are slightly increased compared to the baseline ensemble (+4%). This sensitivity can be explained by the large-scale phosphorus increase and regional increases in nitrogen and phosphorus concentrations (Figure 10) in the biogeochemical simulation. This sensitivity is expected to be produced by the reduced iron concentrations, which limit the phytoplankton growth and thus the nutrient uptake.

The removal of atmospheric nitrogen deposition ("*noNdepo*") leads to a global decrease in surface nitrogen concentration

345 and an increase in surface phosphorus concentrations across the entire domain (Figure 10). The resulting *Sargassum* coverage is significantly decreased over the whole domain, and the annual averaged stranding decreases by 10% (Figure 9d).

5 Discussion and summary

Since 2011, unprecedented massive stranding of the holopelagic *Sargassum* have been reported on the coasts of the Caribbean Sea, Northern Brazil and West Africa. In this paper we developed an Eulerian model of *Sargassum*, which integrates transport,

350 strandings and algal physiology. The *Sargassum* model is based on the ocean modelling platform NEMO, and is forced by the physical and biogeochemical fields of a regional model (TATL025BIO) as well as by the ERA5 wave and wind fields. An ensemble approach has been used to optimize the physiological parameters. The results demonstrate the ability of the model to represent the spatial distribution and seasonal cycle of the *Sargassum* biomass in the West Atlantic and the Caribbean Sea.

While windage and inertial effects are considered of importance for the drift properties and large scale advection (Brook

355 et al. 2019, Berline et al. 2020, Beron-Vera et al. 2020, Putman et al. 2018, 2020), we show here that Stokes drift has also significant impacts on the distribution of the *Sargassum*, and in particular on their entrance in the Caribbean Sea. In addition to the anomalous currents that may be at the origin of the *Sargassum* bloom in 2011 (Johns et al. 2020), wave drift could also have contributed to the dissemination of the algae toward the Equatorial Atlantic in the early 2010's. Wave transport of algae is therefore an important component of *Sargassum* modelling that has not yet been accounted for in previous modelling efforts

360 (Brooks et al., 2018; Putman et al., 2018; Wang et al., 2019, Johns et al. 2020) and should deserve further attention.

The ability of the model to simulate the large-scale distribution was also used to conduct sensitivity tests on the nutrient forcing from rivers, dust and atmospheric deposition. Here, it is worth remembering that the *Sargassum* model is not coupled with the biogeochemical model so it is not directly forced by these external inputs of nutrients but through the biogeochemical model. This prevents the representation of some opportunistic utilization of nutrients that could be done by the algae. With

365 this limitation in mind, our results evidence that riverine nutrient and atmospheric nutrient inputs could feed the basin scale growth of *Sargassum*, in accordance with various hypothesis in the literature (e.g. Wang et al. 2019). We found a 25% and

Geoscientific
Model Development
Discussions

EGU

10% decrease in annual *Sargassum* distribution in the experiments without river nutrient runoff and without atmospheric nitrogen deposition, respectively. This means that 1) *Sargassum* distribution is sensitive to these forcings, but 2) these forcings alone cannot control the total *Sargassum* biomass. At this stage, the quantification of their role in the interannual variability

370 and overall increase of Sargassum remains an open question that will deserve further attention.

Several aspects which could be of potential importance for *Sargassum* growth have not been considered here. First, growth and mortality could depend on the age of the fragments, through colonization by epiphytes. There is a lack of knowledge on these aspects and mesocosm experiments would be useful to better constrain such dependence in the model, if relevant. Second, we assume that *Sargassum* does not compete with phytoplankton for resources. How much this hypothesis is valid remains an

375 open question. The *Sargassum* coverage per area of 0.5×0.5° is rarely above 0.1% (*e.g.* Wang et al. 2019). So, at regional scale, it seems reasonable to consider that *Sargassum* growth does not affect phytoplankton growth. But at the local scale (scale of a raft) and particularly with low mixing conditions, *Sargassum* could compete with phytoplankton for resources. A full coupling of our *Sargassum* model with PISCES-Q may allow us to address such questions. Third, our results show a strong dependence on the nitrogen uptake parameters. We do not consider possible fixation of atmospheric N through diazotrophic

380 assemblage. Biological nitrogen fixation by diazotrophic macroalgal association has been shown to be important for some *Sargassum* species (e.g. *Sargassum horneri*, Raut et al. 2018) and this could also be the case for the holopelagic *Sargassum* where epibionts N-fixating bacteria have been observed on these species (Carpenter 1972, Michotey et al. 2020).

Finally, our modelling system succeeds in maintaining some biomass in the Central and Eastern Tropical Atlantic. This pool of *Sargassum* has been shown to be of key importance in the year-to-year maintenance of the population (Wang et al.

385 2019). So, we expect the model to be useful to address the question of interannual variations.

390 **Data availability**

The Sargassum model is built upon the standard NEMO code (release 4.0.1, rev 11533). The reference code can be downloaded from the NEMO website (http://www.nemo-ocean.eu/, last access: 11 September 2019). The NEMO code modified to include the Sargassum physiology and transport is available in the Zenodo archive (Jouanno and Benshila 2020, http://doi.org/10.5281/zenodo.4275901). Forcing fields for year 2017 are also included in the Zenodo archive.

395

Geoscientific
Model Development
Discussions

Author Contribution

JJ and RB developed the model code, with inputs from LB, FD, TC, JS, CC on the Sargassum modelling strategy. FD, TT, TC provided insight on the Sargassum physiology. SB, OA, CE and MER participated to the physical-biogeochemical model implementation and tuning. LB provided the Sargassum satellite detection product. PN and MM provided fields of atmospheric 400 nitrogen deposition. JJ and AS performed the simulations and analysis. JJ prepared the manuscript with contributions from all co-authors.

405 **References**

Aumont, O. and Bopp, L (2006). Globalizing results from ocean in- situ iron fertilization experiments, Global Biogeochem. Cy., 20, GB2017, https://doi.org/10.1029/2005GB002591.

Aumont, O., Ethé, C., Tagliabue, A., Bopp, L., and Gehlen, M. (2015). PISCES-v2: an ocean biogeochemical model for carbon and ecosystem studies, Geosci. Model Dev., 8, 2465–2513, https://doi.org/10.5194/gmd-8-2465-2015, 2015.

410 Axell, L. B. (2002). Wind-driven internal waves and Langmuir circulations in a numerical ocean model of the southern Baltic Sea. Journal of Geophysical Research: Oceans, 107(C11), 25-1.

Baker, P., Minzlaff, U., Schoenle, A., Schwabe, E., Hohlfeld, M., Jeuck, A., ... & Frutos, I. (2018). Potential contribution of surface-dwelling Sargassum algae to deep-sea ecosystems in the southern North Atlantic. Deep Sea Research Part II: Topical Studies in Oceanography, 148, 21-34.

415 Bendoricchio, G., Coffaro, G., & De Marchi, C. (1994). A trophic model for Ulva rigida in the Lagoon of Venice. Ecological Modelling, 75, 485-496.

Berline, L., Ody, A., Jouanno, J., Chevalier, C., André, J. M., Thibaut, T., & Ménard, F. (2020). Hindcasting the 2017 dispersal of Sargassum algae in the Tropical North Atlantic. Marine Pollution Bulletin, 158, 111431.

Bernard, D., Biabiany, E., Sekkat, N., Chery, R., Cécé, R., 2019. Massive stranding of pelagic sargassum seaweeds on the 420 french Antilles coasts : Analysis of observed situations with Operational Mercator global ocean analysis and forecast system. https://doi.org/10.13142/RG.2.2.32251.7000

Beron-Vera, F. J., & Miron, P. (2020). A minimal Maxey–Riley model for the drift of Sargassum rafts. J. Fluid Mech.

Brooks, M. T., Coles, V. J., Hood, R. R., & Gower, J. F. (2018). Factors controlling the seasonal distribution of pelagic Sargassum. Marine Ecology Progress Series, 599, 1-18.

425 Brooks, M. T., Coles, V. J., & Coles, W. C. (2019). Inertia influences pelagic sargassum advection and distribution. Geophysical Research Letters, 46(5), 2610-2618.

Geoscientific
Model Development
Discussions

Butler JN, Morris BF, Cadwallader J, Stoner AW (1983) Studies of Sargassum and the Sargassum community. Bermuda Biological Station for Research St Georges 22.

Carpenter, E. J. (1972). Nitrogen fixation by a blue-green epiphyte on pelagic Sargassum. Science, 178(4066), 1207-1209.

430   Carpenter, E. J., & Cox, J. L. (1974). Production of pelagic Sargassum and a blue-green epiphyte in the western Sargasso Sea 1. Limnology and Oceanography, 19(3), 429-436.

Decharme, B., Delire, C., Minvielle, M., Colin, J., Vergnes, J. P., Alias, A., Saint-Martin, D, Séférian, R.; Sénési, S., and Voldoire, A. (2019). Recent changes in the ISBA-CTRIP land surface system for use in the CNRM-CM6 climate model and in global off-line hydrological applications. Journal of Advances in Modeling Earth Systems, 11(5), 1207-1252.

435   Deutsch, J. L., & Deutsch, C. V. (2012). Latin hypercube sampling with multidimensional uniformity. Journal of Statistical Planning and Inference, 142(3), 763-772.

Drugé, T., Nabat, P., Mallet, M., and Somot, S. (2019) Model simulation of ammonium and nitrate aerosols distribution in the Euro-Mediterranean region and their radiative and climatic effects over 1979–2016, Atmos. Chem. Phys., 19, 3707-3731, DOI:10.5194/acp-19-3707-2019.

440   Dussin, R., Barnier, B., and Brodeau, L.: The making of Drakkar forcing set DFS5, DRAKKAR/MyOcean Report 01-04-16, LGGE, Grenoble, France, 2016.

Garcia, H. E., Locarnini, R. A., Boyer, T. P., Antonov, J. I., Zweng, M. M., Baranova, O. K., and Johnson, D. R.: World Ocean Atlas 2009, Volume 4: Nutrients (phosphate, nitrate, silicate), S. Lev- itus, Ed. NOAA Atlas NESDIS 71, U.S. Government Printing Office, Washington, D.C., 398 pp., 2010.

445   García-Sánchez, M., Graham, C., Vera, E., Escalante-Mancera, E., Álvarez-Filip, L., & van Tussenbroek, B. I. (2020). Temporal changes in the composition and biomass of beached pelagic Sargassum species in the Mexican Caribbean. Aquatic Botany, 167, 103275.

Giffard, P., Llovel, W., Jouanno, J., Morvan, G., & Decharme, B. (2019). Contribution of the Amazon River discharge to regional sea level in the tropical Atlantic Ocean. Water, 11(11), 2348.

450   Hanisak, M.D. (1983). The nitrogen relationship of marine macroalgae. In: ed. E.J. Carpenter and D.G. Capone, Nitrogen in the Marine Envinroment. Academic Press, New York: pp. 699-730.

Hanisak, M. D., & Samuel, M. A. (1987). Growth rates in culture of several species of Sargassum from Florida, USA. In Twelfth International Seaweed Symposium (pp. 399-404). Springer, Dordrecht.

Hanson, R. B. (1977). Pelagic Sargassum community metabolism: Carbon and nitrogen. *Journal of Experimental Marine*
455   *Biology and Ecology*, *29*(2), 107-118.

Hernandez O., J. Jouanno, V. Echevin, and O. Aumont (2017). Impacts of chlorophyll concentrations on the Tropical Atlantic Ocean. J. Geophys. Res. Oceans, doi:10.1002/2016JC012330.

Hernandez, O. , J. Jouanno and F. Durand (2016). Do the Amazon and Orinoco river plumes influence tropical cyclone-induced surface cooling. Journal of Geophysical Research: Oceans, 121(4), 2119-2141.

460 Howard, K. L., and Menzies, R. J. (1969). Distribution and production of Sargassum in the waters off the Carolina coast. Botanica Marina, 12(1-4), 244-254.

Johns, E. M., R. Lumpkin, N. F. Putman, R. H. Smith, F. E. Muller-Karger, D. Rueda, C. Hu, M. Wang, M. T. Brooks, L. J. Gramer, F. E. Werner (2020). The establishment of a pelagic Sargassum population in the tropical Atlantic: biological consequences of a basin-scale long distance dispersal event. Progress in Oceanography,
465 doi.org/10.1016/j.pocean.2020.102269.

Johnson, D.L., Richardson, P.L., 1977. On the wind-induced sinking of Sargassum. Journal of Experimental Marine Biology and Ecology 28, 255-267. doi: 10.1016/0022-0981(77)90095-8.

Jouanno J., and Benshila R. (2020, November 16). Sargassum distribution model based on the NEMO ocean modelling platform (Version 0.0). Zenodo. http://doi.org/10.5281/zenodo.4275901.

470 Kwiatkowski, L., Aumont, O., Bopp, L., & Ciais, P. (2018). The Impact of variable Phytoplankton Stoichiometry on Projections of primary production, food quality, and carbon uptake in the global ocean. Global Biogeochemical Cycles, 32(4), 516-528.

Langin (2018). Seaweed masses assault Caribbean islands. Science, 360(6394), 1157–1158.

Lapointe, B. E. (1986). Phosphorus-limited photosynthesis and growth of Sargassum natans and Sargassum fluitans
475 (Phaeophyceae) in the western North Atlantic. Deep Sea Research Part A. Oceanographic Research Papers, 33(3), 391-399.

Lapointe, B. E. (1995). A comparison of nutrient-limited productivity in Sargassum natans from neritic vs. oceanic waters of the western North Atlantic Ocean. Limnology and Oceanography, 40(3), 625-633.

Lapointe BE, West LE, Sutton TT, Hu C (2014).Ryther revis- ited: Nutrient excretions by fishes enhance productivity of pelagic Sargassum in the western North Atlantic Ocean. J Exp Mar Biol Ecol 458:46−56.

480 Langmuir, I. (1938). Surface motion of water induced by wind. Science 87, 119–123.

Large, W. G. and Yeager, S. (2009). The global climatology of an interan- nually varying air-sea flux data set, Clim. Dynam., 33, 341–364, https://doi.org/10.1007/s00382-008-0441-3, 2009.

Lehman, J.T., Botkin, D.B., Likens, G.E. (1975). The assumptions and rationales of a computer model of phytoplankton population dynamics. Limnology and Oceanography 20 (3), 343–364.

485 Louime, C., Fortune, J., Gervais, G., 2017. Sargassum Invasion of Coastal Environments: A Growing Concern. Am. J. Environ. Sci. 13, 58–64. https://doi.org/10.3844/ajessp.2017.58.64.

Madec G, the NEMO team (2016) NEMO ocean engine. Note du Pôle de modélisation, Institut Pierre-Simon Laplace (IPSL), France 27:1288–1619

Maréchal, J. P., Hellio, C., & Hu, C. (2017). A simple, fast, and reliable method to predict Sargassum washing ashore in the
490 Lesser Antilles. Remote Sensing Applications: Society and Environment, 5, 54-63.

Martins, I., & Marques, J. C. (2002). A model for the growth of opportunistic macroalgae (Enteromorpha sp.) in tidal estuaries. Estuarine, Coastal and Shelf Science, 55(2), 247-257.

Michotey, V., Blanfuné, A., Chevalier, C., Garel, M., Diaz, F., Berline, L., ... & Changeux, T. (2020). In situ observations and modelling revealed environmental factors favouring occurrence of Vibrio in microbiome of the pelagic Sargassum responsible

495   for strandings. Science of the Total Environment, 748, 141216.

Michou, M., P. Nabat, D. Saint-Martin, J. Bock, B. Decharme, M. Mallet, R. Roehrig, R. Séférian, S. Sénési and A. Voldoire (2020) Present-day and historical aerosol and ozone characteristics in CNRM CMIP6 simulations, JAMES, 12, e2019MS001816, DOI:10.1029/2019MS001816.

Ody, A., Thibaut, T., Berline, L., Changeux, T., André, J. M., Chevalier, C., ... & Connan, S. (2019). From In Situ to satellite

500   observations of pelagic Sargassum distribution and aggregation in the Tropical North Atlantic Ocean. PloS one, 14(9), e0222584.

Olsen, A., R. M. Key, S. van Heuven, S. K. Lauvset, A. Velo, X. Lin, C. Schirnick, A. Kozyr, T. Tanhua, M. Hoppema, S. Jutterström, R. Steinfeldt, E. Jeansson, M. Ishii, F. F. Pérez and T. Suzuki. The Global Ocean Data Analysis Project version 2 (GLODAPv2) – an internally consistent data product for the world ocean, Earth Syst. Sci. Data, 8, 297–323, 2016,

505   doi:10.5194/essd-8-297-2016.

Oviatt, C. A., Huizenga, K., Rogers, C. S., & Miller, W. J. (2019). What nutrient sources support anomalous growth and the recent sargassum mass stranding on Caribbean beaches? A review. Marine pollution bulletin, 145, 517-525.

Oyesiku, O. O., & Egunyomi, A. (2014). Identification and chemical studies of pelagic masses of Sargassum natans (Linnaeus) Gaillon and S. fluitans (Borgessen) Borgesen (brown algae), found offshore in Ondo State, Nigeria. African Journal of

510   Biotechnology, 13(10).

Perrot, T., Rossi, N., Ménesguen, A., & Dumas, F. (2014). Modelling green macroalgal blooms on the coasts of Brittany, France to enhance water quality management. Journal of Marine Systems, 132, 38-53.

Prospero, J. M., Barkley, A. E., Gaston, C. J., Gatineau, A., Campos y Sansano, A., & Panechou, K. (2020). Characterizing and quantifying African dust transport and deposition to South America: Implications for the phosphorus budget in the Amazon

515   Basin. Global Biogeochemical Cycles, 34, e2020GB006536. https://doi.org/ 10.1029/2020GB006536

Putman N.F., Goni G.J., Gramer L.J., Hu C., Johns E.M., Trinanes J., et al. (2018). Simulating transport pathways of pelagic Sargassum from the Equatorial Atlantic into the Caribbean Sea. Progress in Oceanography, 165, 205–214.

Putman, N. F., Lumpkin, R., Olascoaga, M. J., Trinanes, J., & Goni, G. J. (2020). Improving transport predictions of pelagic Sargassum. Journal of Experimental Marine Biology and Ecology, 529, 151398.

520   Radenac, M.-H., Jouanno, J., Tchamabi, C. C., Awo, M., Bourlès, B., Arnault, S., and Aumont, O. (2020). Physical drivers of the nitrate seasonal variability in the Atlantic cold tongue. Biogeosciences, 17, 529–545.

Raut, Y., Morando, M., & Capone, D. G. (2018). Diazotrophic Macroalgal Associations With Living and Decomposing Sargassum. Frontiers in Microbiology, 9, 3127.

Ren, J. S., Barr, N. G., Scheuer, K., Schiel, D. R., & Zeldis, J. (2014). A dynamic growth model of macroalgae: application in
525 an estuary recovering from treated wastewater and earthquake-driven eutrophication. Estuarine, Coastal and Shelf
Science, 148, 59-69.

Schell, J. M., Goodwin, D. S., & Siuda, A. N. (2015). Recent Sargassum inundation events in the Caribbean: shipboard
observations reveal dominance of a previously rare form. Oceanography, 28(3), 8-11.

Schoener, A., Rowe, G.T., 1970, Pelagic Sargassum and its presence among the deep-sea benthos. Deep-Sea Research 17,
530 923-925. doi: 10.1016/0011-7471(70)90010-0.

Séférian, R., Berthet, S., Yool, A. et al. Tracking Improvement in Simulated Marine Biogeochemistry Between CMIP5 and
CMIP6. Curr Clim Change Rep 6, 95–119 (2020). https://doi.org/10.1007/s40641-020-00160-0.

Sissini, M. N., de Barros Barreto, M. B. B., Széchy, M. T. M., de Lucena, M. B., Oliveira, M. C., Gower, J., G. Liu, E. de
Oliveira Bastos, D. Milstein, F. Gusmão, J.E. Martinelli-Filho (2017). The floating Sargassum (Phaeophyceae) of the South
535 Atlantic Ocean–likely scenarios. Phycologia, 56, pp. 321-328.

Smetacek, V., & Zingone, A. (2013). Green and golden seaweed tides on the rise. Nature, 504(7478), 84-88.

Solidoro, C., Pecenik, G., Pastres, R., Franco, D., & Dejak, C. (1997). Modelling macroalgae (Ulva rigida) in the Venice
lagoon: Model structure identification and first parameters estimation. Ecological Modelling, 94(2-3), 191-206.

Storto, A., Masina, S., Simoncelli, S., Iovino, D., Cipollone, A., Drevillon, M., Drillet, Y., von Schuckman, K., Parent, L. Gar-
540 ric, G., Greiner, E., Desportes, C., Zuo, H., Balmaseda, M. A., and Peterson, K. A.: The added value of the multi-system spread
information for ocean heat content and steric sea level investigations in the CMEMS GREP ensemble reanalysis prod- uct,
Clim. Dynam., 53, 287, https://doi.org/10.1007/s00382-018- 4585-5, 2018.

SO-Hybam, 2019. Observation Service SO HYBAM Geodynamical, hydrological and biogeochemical control of
erosion/alteration and material transport in the Amazon, Orinoco and Congo basins. so-hybam.org. Last access, november
545 2019.

Wang M. and Hu C. (2016) Mapping and quantifying Sargassum distribution and coverage in the Central Western Atlantic
using MODIS observations. Remote Sensing of Environment. 183. Pp. 350-367.

Wang M. and Hu C. (2017). Predicting Sargassum blooms in the Caribbean Sea from MODIS observations. Geophysical
Research Letters, 44: 3265–3273.

550 Wang, M., Hu, C., Cannizzaro, J., English, D., Han, X., Naar, D., B. Lapointe, R. Brewton, and F. Hernandez (2018). Remote
sensing of Sargassum biomass, nutrients, and pigments. Geophysical Research Letters, 45, 12,359–12,367. https://doi.org/
10.1029/2018GL078858

Wang, M., Hu, C., Barnes, B. B., Mitchum, G., Lapointe, B., & Montoya, J. P. (2019). The great Atlantic Sargassum
belt. Science, 365(6448), 83-87.

555 Woodcock, A.H., (1993). Winds subsurface pelagic Sargassum and Langmuir circulations. Journal of Experimental Marine
Biology and Ecology 170, 117-125. doi: 10.1016/0022-0981(93)90132- 8.

Zhong, Y., Bracco, A., & Villareal, T. A. (2012). Pattern formation at the ocean surface: Sargassum distribution and the role of the eddy field. Limnology and Oceanography: Fluids and Environments, 2(1), 12-2.

560

| Parameter	Description	Parameter range	Parameters for baseline simulation	Unit	Reference
μ_{max}	Maximum uptake rate of carbon	[0.05-0.09]	0.069	d^{-1}	Lapointe et al. (2014)
I_{opt}	Optimal light intensity	[60-80]	72.7	$W\ m^{-2}$	Hanisak and Samuel (1987), Lapointe et al. (1995)
K_N	Half saturation constant for N uptake (NO3+NH4)	[0.001-0.01]	0.0014	$mmol\ m^{-3}$	This study
K_P	Half saturation constant for P uptake (PO4)	[0.001-0.01]	0.0044	$mmol\ m^{-3}$	This study
Tmin	Lower temperature limit below which growth ceases,	[10 – 14]	10.8	°C	Hanisak and Samuel (1987)
Tmax	Upper temperature limit above which growth ceases	[40 – 50]	43.2	°C	This study.
Topt	Optimum temperature at which growth is maximum	[22-28]	26.0	°C	Hanisak and Samuel (1987)
m	Maximum mortality rate	[0.05-0.1]	0.04	d^{-1}	This study
m_{LC}	Maximum sinking rate	[0.05 - 0.1]	0.0.057	d^{-1}	This study
λ_m	Coefficient of the exponential slope for mortality dependance to temperature	[0.2 – 0.7]	0.62		This study
λm_{LC}	Coefficient of the exponential slope for Langmuir mortality to depth	[0.2 - 0.7]	0.28		This study
V_{Nmax}	Nitrogen maximum uptake rate	[5 10^{-4} – 3 10^{-3}]	1.23 10^{-3}	$mgN\ (mgC)^{-1}\ d^{-1}$	Lapointe et al. (1995)
V_{Pmax}	Phosphorus maximum uptake rate	[9 10^{-5} – 7 10^{-4}]	3.78 10^{-4}	$mgP\ (mgC)^{-1}\ d^{-1}$	Lapointe et al. (1995)
Q_{Nmin}	Minimum N quota	[0.033 – 0.058]	0.028	$mgN\ (mgC)^{-1}$	Lapointe et al. (1995)
Q_{Nmax}	Maximum N quota	[0.016 – 0.029]	0.035	$mgN\ (mgC)^{-1}$	Lapointe et al. (1995)
Q_{Pmin}	Minimum P quota	[0.0025 – 0.0035]	0.003	$mgP\ (mgC)^{-1}$	Lapointe et al. (1995)
Q_{Pmax}	Maximum P quota	[0.005 – 0.0125]	0.011	$mgP\ (mgC)^{-1}$	Lapointe et al. (1995)
Windage	Direct wind effect on the *Sargassum* raft displacement	[0 – 1.5]	1.12	%	Berline et al. (2020), Putman et al. (2020)

Table 1. *Sargassum* model parameters.
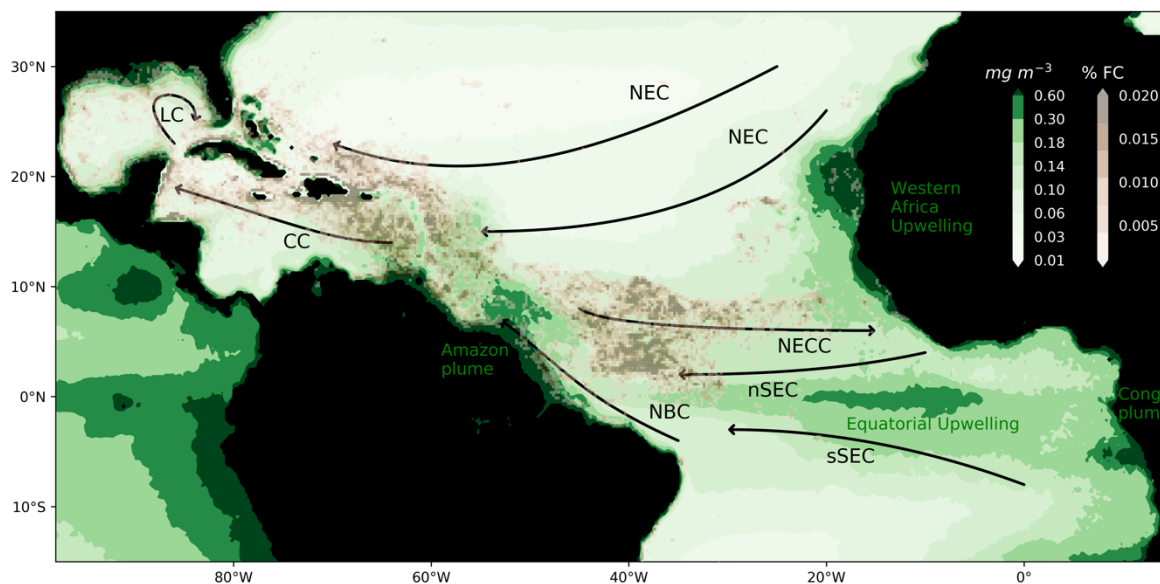
Figure 1. *Sargassum* fractional coverage obtained from MODIS in July-August 2017 (Berline et al. 2020, brown color scale; value between 0.001 and 0.02%) and surface chlorophyll distribution in July-August (green color scale; im mg m^{-3}) based on GlobColour MODIS monthly product from 2010 to 2018. Circulation schematic of the surface currents is superimposed: the North Equatorial Current (NEC), the northern and southern branches of the South Equatorial Current (nSEC and sSEC), the North Equatorial Countercurrent (NECC), the North Brazil Current (NBC), the Caribbean Current (CC), and the Loop Current (LC).
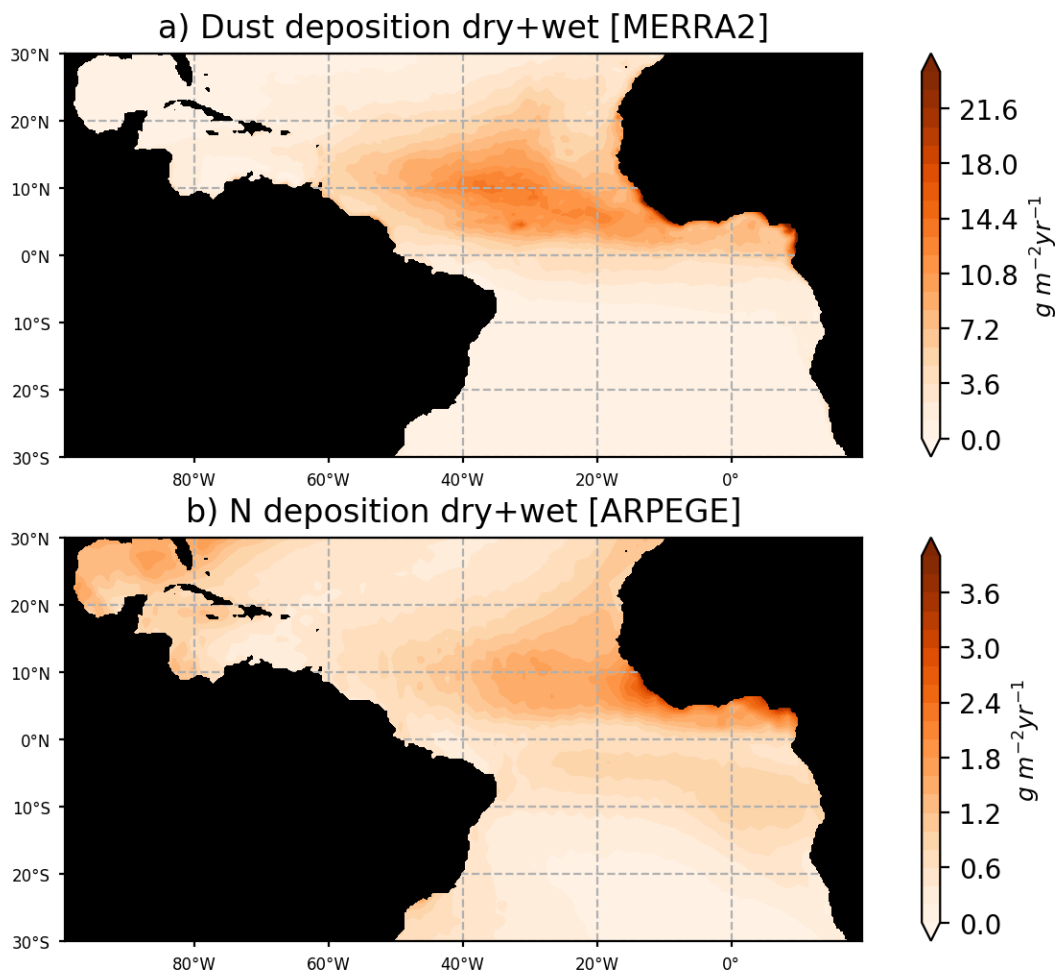
Figure 2. Dust fluxes to the ocean from MERRA2 reanalysis for year 2017 (a), and nitrogen flux to the ocean from ARPEGE simulations averaged over the period 2010-2014. Nitrogen fluxes consider the dry and wet fluxes at the ocean surface of NO_3, NH_4 and NH_3. Dust fluxes consider the total dust dry-plus-wet deposition product (DUDPWTSUM) from MERRA2.
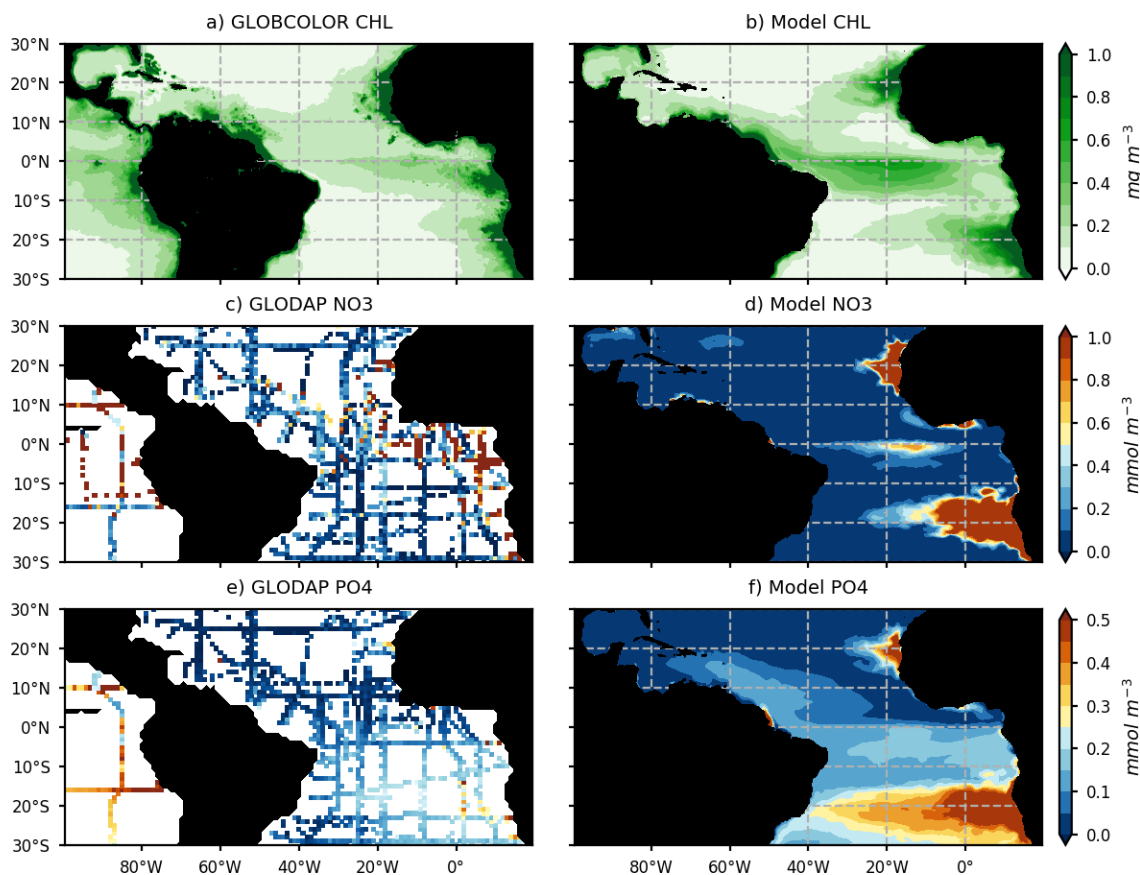
Figure 3. Annual mean surface chlorophyll concentrations (mg chl-a m^{-3}) from Globcolour satellite product (a) and model (b) for year 2017. Spatial distribution of surface NO_3 and PO_4 concentration (c,e ; mmol m^{-3}) from historical cruises of the GLODAPv2_2016 database (https://www.nodc.noaa.gov/ocads/oceans/GLODAPv2/) and annual mean surface NO_3 and PO_4 distribution from the model (d,f).
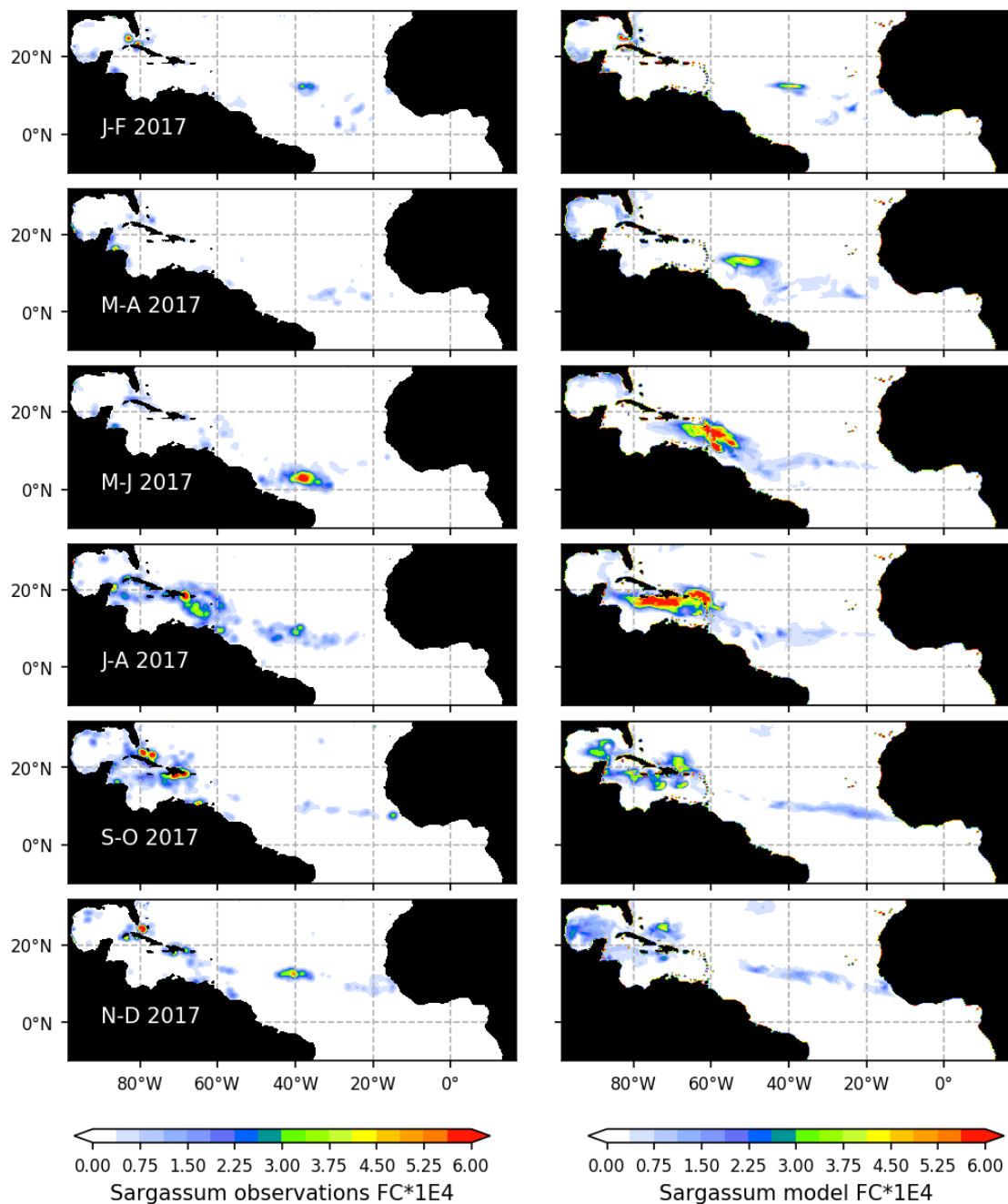
Figure 4. Seasonal distribution of *Sargassum* Fractional Coverage for year 2017 from observations (left) and from a selected ensemble of 100 simulations (Ω_{100}) with varying parameters (right).
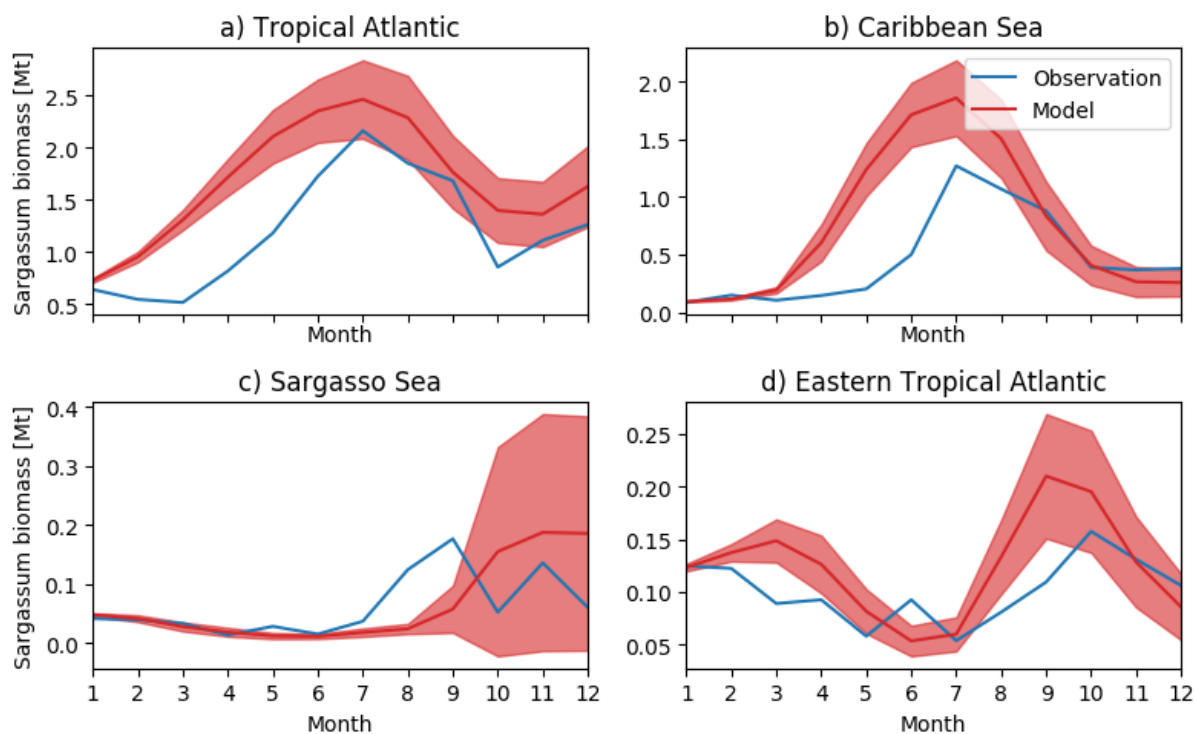
Figure 5. Seasonal distribution of *Sargassum* Fractional Coverage for year 2017 from observations (blue) and from a selected ensemble of 100 simulations (Ω_{100}) with varying parameters (mean in red and variance in shaded red) averaged in different areas: (a) Tropical Atlantic [98°W-10°W;0°N-30°N], (b) Caribbean Sea [85°W-55°W;8°N-22°N], (c) Sargasso Sea [80°W-50°W;23°N-30°N], and Eastern North Tropical Atlantic [30°W-0°E;0°N-15°N].
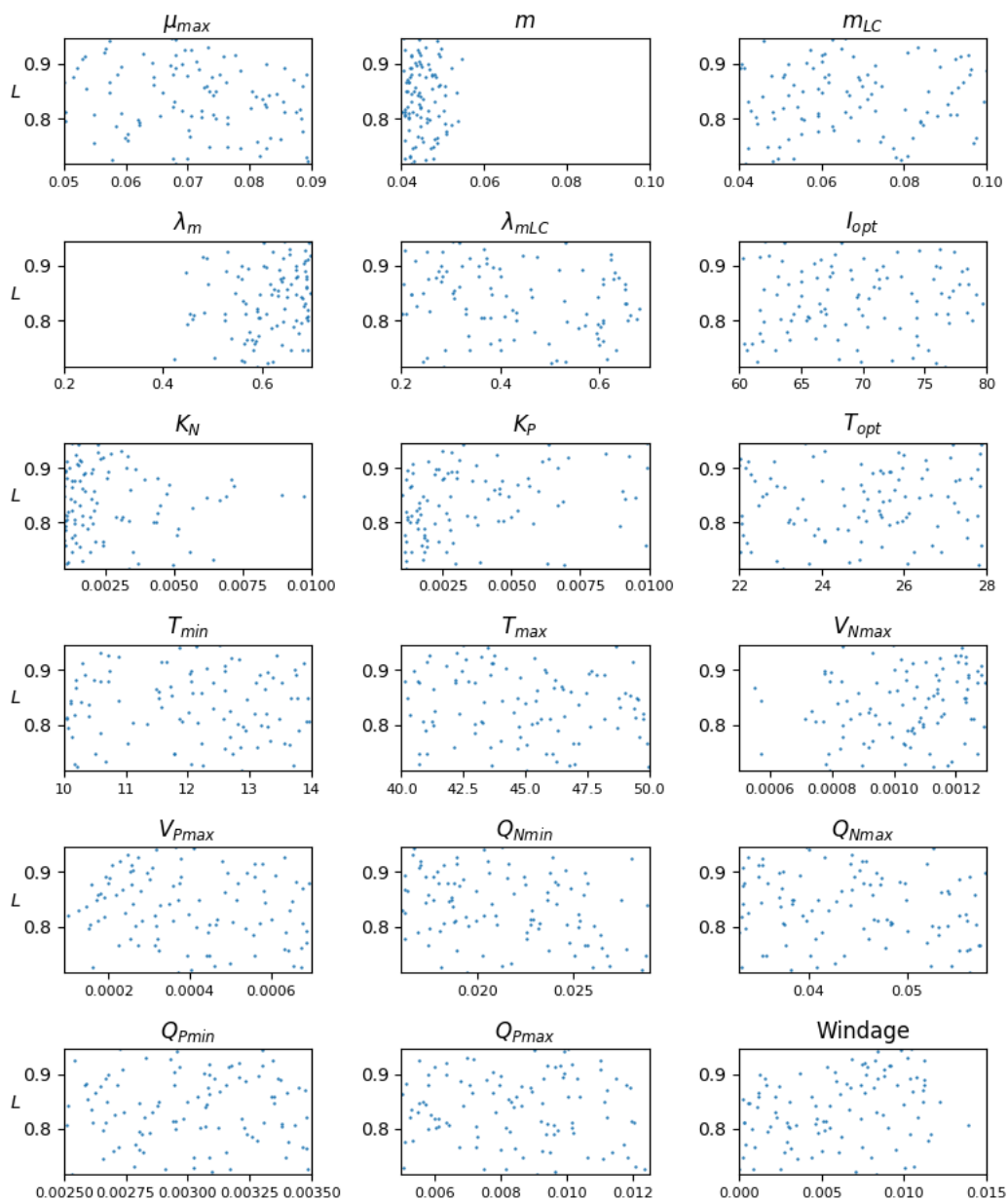
Figure 6. Likelihood (L) as a function of the different parameters that have been varied in the optimization experiment, shown here for the ensemble Ω_{100} that composes the ensemble averages in Figures 4 and 5. Units are given in Table 1.
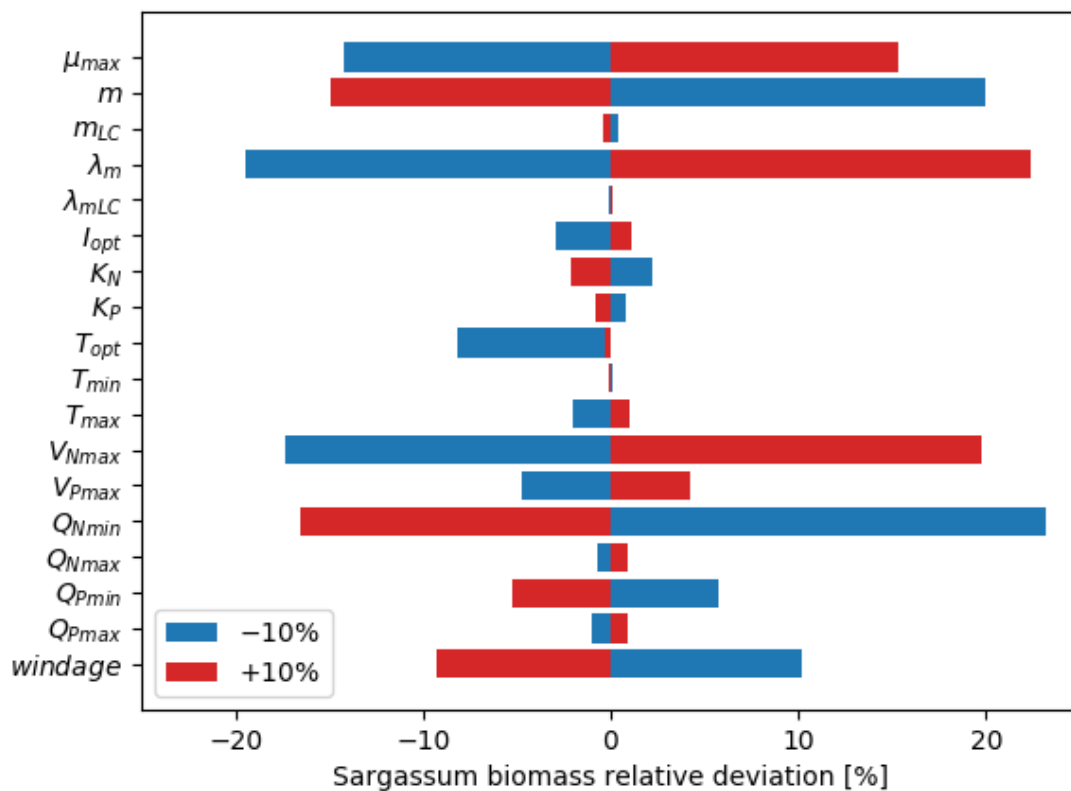
Figure 7. Sensitivity analysis to model parameters expressed as the mean relative deviation (%) between the baseline simulation and the simulation in which one parameter was modified by ±10%. The set of parameters for the baseline simulation are given in Table 1.
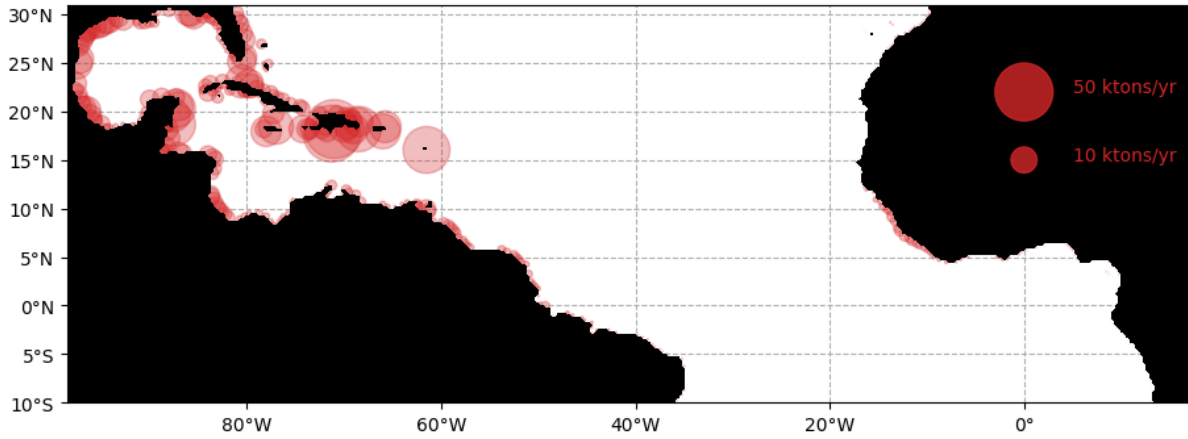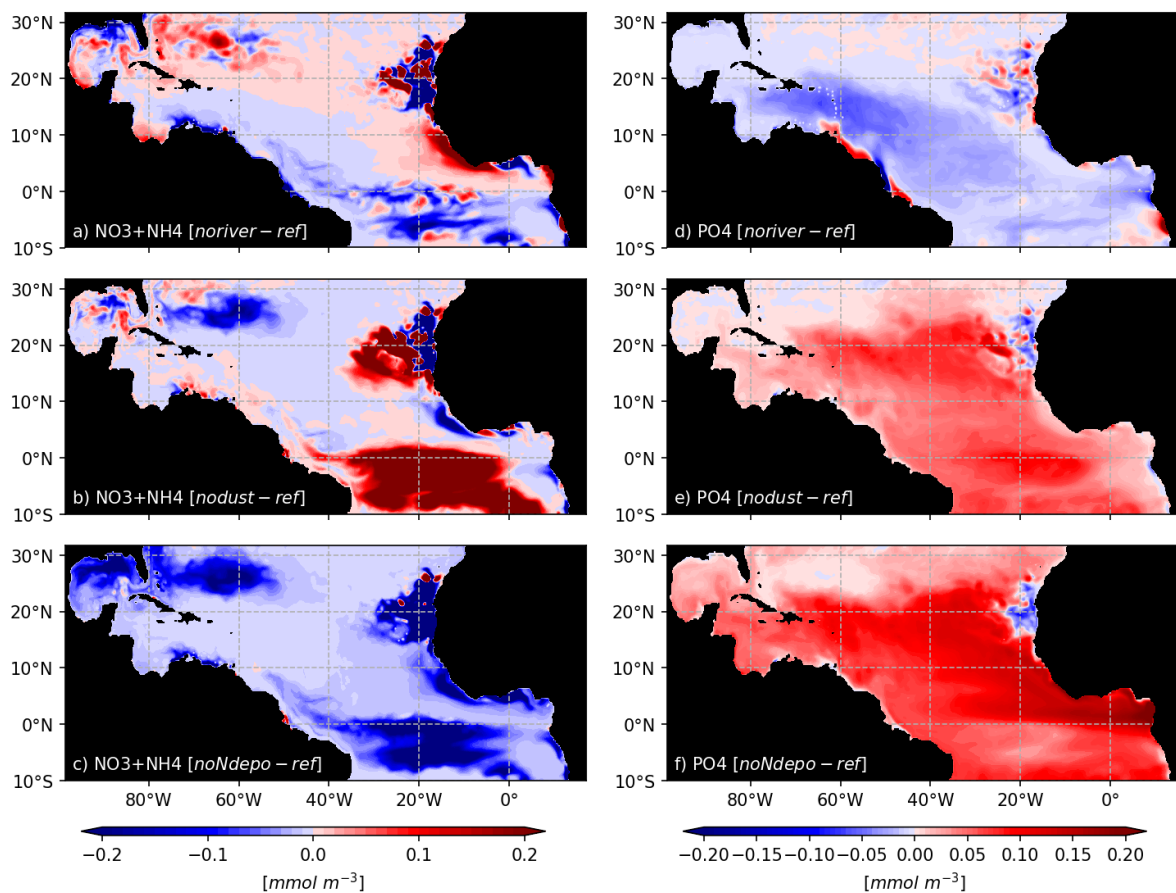
600

Figure 8. Cumulated annual *Sargassum* wet biomass stranding per area of 25x25km for year 2017 obtained from the ensemble Ω_{100}.

Geoscientific
Model Development
Discussions
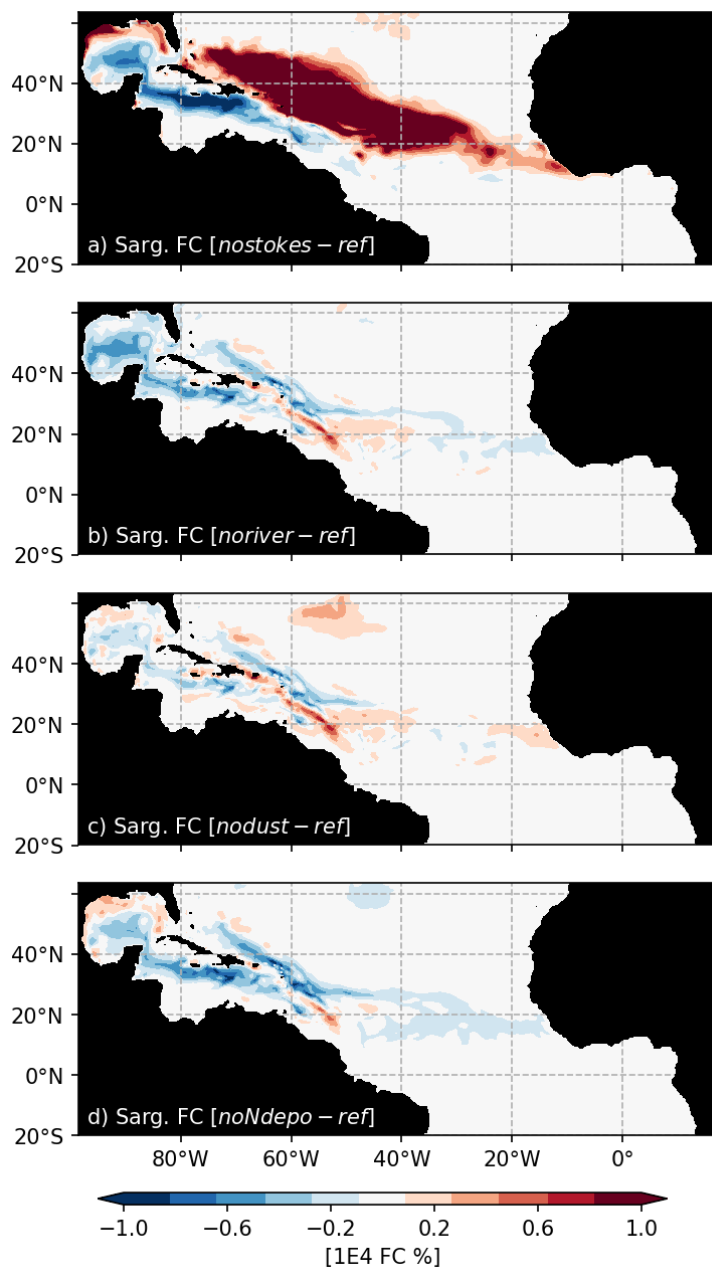
Fig. 9. Ensemble anomalies of *Sargassum* coverage (in % of surface) from sensitivity ensemble simulations of 100 members each, which were performed with the set of parameters from Ω_{100}.

Fig. 10. Biogeochemical response to sensitivity experiments to river, dust and N deposition: surface anomalies of $NO_3 + NH_4$ (left) and PO_4 (right) with respect to the reference TATL025BIO simulation.